

# MHD instabilities at the disk-magnetosphere boundary: 3D simulations

Akshay K. Kulkarni and Marina M. Romanova

Department of Astronomy, Cornell University, Ithaca, NY 14853, USA  
email:{akshay,romanova}@astro.cornell.edu

**Abstract.** We present results of 3D simulations of MHD instabilities at the accretion disk-magnetosphere boundary. The instability is Rayleigh-Taylor, and develops for a large range of parameter values. It manifests itself in the form of tall, thin tongues of plasma that reach the star by penetrating through the magnetosphere in the equatorial plane. The tongues rotate around the star in the equatorial plane, and their shape and number changes with time on inner-disk dynamical timescales. In contrast with funnel flows, which deposit matter mainly in the polar region, the tongues deposit matter much closer to the stellar equator.

**Keywords.** Accretion, accretion disks, instabilities, (magnetohydrodynamics:) MHD, stars: circumstellar matter, stars: magnetic fields, stars: oscillations, stars: pre-main-sequence, stars: rotation, stars: spots.

---

## 1. Introduction

The geometry of the accretion flow around magnetized stars is a problem of long-standing interest. It is an important factor in determining the observed spectral and variability properties of the accreting system. An accretion disk around a magnetized central object is truncated approximately at the distance from the central star where the magnetic energy density becomes comparable to the matter energy density. Beyond that point, there are two ways in which the gas can accrete to the star: (1) through funnels, or magnetospheric accretion (Ghosh & Lamb 1978, 1979); (2) through plasma instabilities at the disk-magnetosphere interface (Arons & Lea 1976; Elser & Lamb 1977; Spruit & Taam 1990; Rastätter & Schindler 1999; Li & Narayan 2004). Two- and three-dimensional simulations have shown accretion through funnel streams (Romanova *et al.* 2002, 2003, 2004; Kulkarni & Romanova 2005). Plasma instabilities at the disk-magnetosphere interface, when present, will completely alter the geometry of the accretion flow. In general, the Rayleigh-Taylor instability is expected to develop at the disk-magnetosphere interface because of the high-density disk matter being supported by the low-density magnetospheric plasma. The Kelvin-Helmholtz instability is also expected to develop because of the discontinuity in the angular velocity of the matter at the boundary. The inner disk matter is expected to rotate at the local Keplerian velocity, while the magnetospheric plasma corotates with the star. There have been numerous studies of the development of such instabilities.

We report on the discovery of instabilities at the disk-magnetosphere interface in full three-dimensional simulations of disk accretion to a magnetized star. The instabilities occur for a large range of parameter values. We discuss our numerical model in § 2, and present our results in § 3.

## 2. The numerical model

The model we use is the same as in our earlier 3D MHD simulations (Koldoba *et al.* 2002; Romanova *et al.* 2003, 2004). The star has a dipole magnetic field, the axis of which makes an angle  $\Theta$  with the star's rotation axis. The rotation axes of the star and the accretion disk are aligned. There is a low-density corona around the star and the disk which also rotates about the same axis. To model stationary accretion, the disk is chosen to initially be in a quasi-equilibrium state, where the gravitational, centrifugal and pressure gradient forces are in balance (Romanova *et al.* 2002). Viscosity is modelled using the  $\alpha$ -model (Shakura & Sunyaev 1973; Novikov & Thorne 1973). To model accretion, the ideal MHD equations are solved numerically in three dimensions, using a Godunov-type numerical code, written in a "cubed-sphere" coordinate system rotating with the star (Koldoba *et al.* 2002; Romanova *et al.* 2003). The boundary conditions at the star's surface amount to assuming that the infalling matter passes through the surface of the star. So the dynamics of the matter after it falls on the star is ignored. The inward motion of the accretion disk is found to be stopped by the star's magnetosphere at the Alfvén radius, where the magnetic and matter energy densities become equal. The subsequent evolution depends on the parameters of the model.

The simulations are done using the following dimensionless variables: the radial coordinate  $r' = r/R_0$ , the fluid velocity  $\mathbf{v}' = \mathbf{v}/v_0$ , the density  $\rho' = \rho/\rho_0$ , the magnetic field  $\mathbf{B}' = \mathbf{B}/B_0$ , the pressure  $p' = p/p_0$ , the temperature  $T' = T/T_0$ , and the time  $t' = t/t_0$ . The variables with subscript 0 are dimensional reference values and the unprimed variables are the dimensional variables. Because of the use of dimensionless variables, the results are applicable to a wide range of objects and physical conditions, each with its own set of reference values. To apply our simulation results to a particular situation, we have the freedom to choose three parameters, and all the reference values are calculated from those. We choose the mass, radius and surface magnetic field of the star as the three independent parameters.

For protostars, we take the mass of the star to be  $M = 0.8M_\odot = 1.6 \times 10^{33}$  g and its radius  $R = 2R_\odot = 1.4 \times 10^6$  km  $= 1.4 \times 10^{11}$  cm. The reference length scale is  $R_0 = R/0.35 = 4 \times 10^{11}$  cm  $\approx 0.03$  AU. The reference velocity is  $v_0 = 1.6 \times 10^7$  cm s $^{-1}$ . The reference angular velocity is  $\omega_0 = 4 \times 10^{-5}$  s $^{-1}$ . The reference time is  $t_0 = 2.5 \times 10^4$  s  $= 0.3$  days. The reference rotation period is  $P_0 = 1.5 \times 10^5$  s  $= 1.8$  days. The reference surface magnetic field is  $B_{\star_0} = 10^3$  G, which is a typical value for protostars. Then the reference magnetic field is  $B_0 = B_{\star_0} (R/R_0)^3 = 43$  G. The reference density is  $\rho_0 = 7 \times 10^{-12}$  g cm $^{-3}$ . The reference pressure is  $p_0 = 1.8 \times 10^3$  dynes cm $^{-2}$ . The reference temperature is  $T_0 = 1.6 \times 10^6$  K. The reference accretion rate is  $\dot{M}_0 = 1.8 \times 10^{19}$  g s $^{-1} = 2.8 \times 10^{-7} M_\odot$  yr $^{-1}$ .

Subsequently, we drop the primes on the dimensionless variables and show dimensionless values in the figures. The dimensionless time in the remainder of this paper is in units of the Keplerian orbital period  $P_0$  at  $r' = 1$ .

## 3. Simulation results

We chose the following parameters for our main case: misalignment angle  $\Theta = 5^\circ$ , stellar surface magnetic field  $B_\star = 2$ , viscosity parameter  $\alpha = 0.1$ , stellar angular velocity  $\Omega_\star = 0.35$ , initial disk radius  $= 2.1$ .

Fig. 1 shows two views of the accretion flow around the star through instabilities (top row) and two views of a magnetospheric (funnel) flow (bottom row). The growth of unstable perturbations at the disk-magnetosphere boundary results in penetration of the

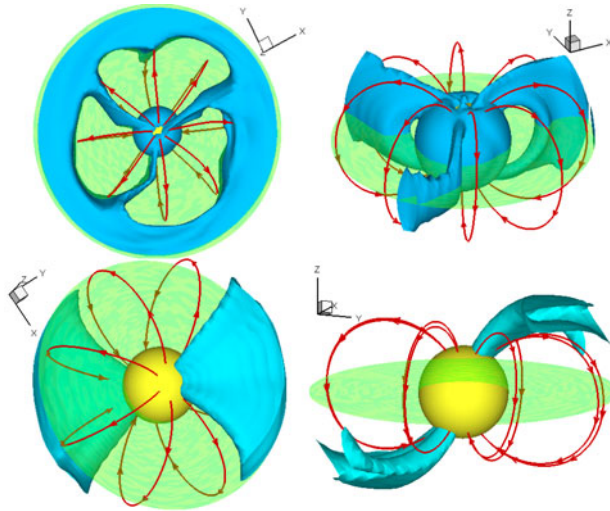


**Figure 1.** Geometry of the accretion flow around a star through instabilities (top row), contrasted with a traditional funnel flow (bottom row). A constant density surface is shown. The lines are magnetospheric magnetic field lines. The translucent disc denotes the equatorial plane. The star's rotational axis is in the  $z$ -direction.

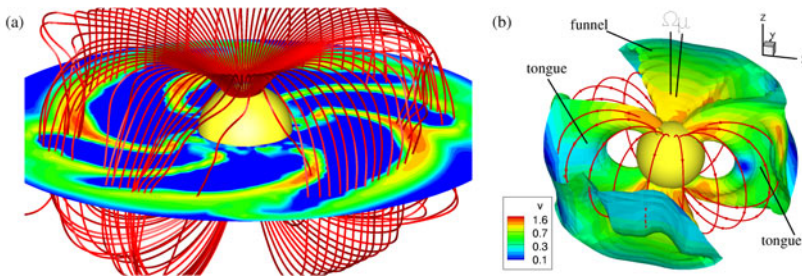


**Figure 2.** (a) A tongue of gas, shown by density contours in the equatorial plane, pushing aside magnetic field lines on its way to the star. Note that the “hole” in the magnetosphere is not artificially depicted – the field lines start out uniformly spaced on the star's surface, and twist aside around the tongue. (b) Cutaway view of the region around the star showing the matter velocity profile in the funnels and tongues, in a reference frame rotating with the star. A constant density surface is shown, overlaid with velocity contours.

magnetosphere by the disk matter, in the form of tongues of gas travelling through the equatorial plane. The tongues are threaded by the magnetic field lines closer to the star and turn into miniature funnel-like flows which deposit matter much closer to the star's equator than true funnel flows do.

The tongues are tall and thin, as opposed to the funnels which are flat and wide. This is because when the tongues penetrate the magnetosphere, they pry the field lines aside (Fig. 2a), since this is energetically more favourable than bending the field lines inward.

The matter velocity profile in the tongues is very similar to that in the funnels, as Fig. 2b shows. It is also seen that the funnels and tongues are not mutually exclusive. We discuss this last point in more detail in § 3.5.

Fig. 3 shows some disk-plane slices of the circumstellar region at various times, in which the tongues are visible. The density enhancements which result in the formation of the tongues can be seen at the base of the tongues. The tongues rotate around the star with the angular velocity of the gas at the inner edge of the disk. This is in contrast

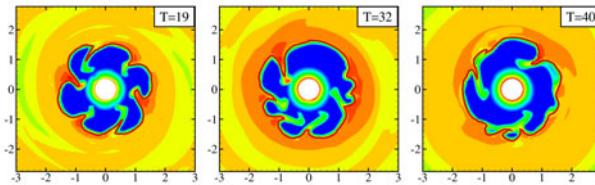


**Figure 3.** Disk-plane slices of the circumstellar region for our main case. The colors represent plasma density contours, ranging from red (highest) to deep blue (lowest). The solid line is the  $\beta = 1$  line.

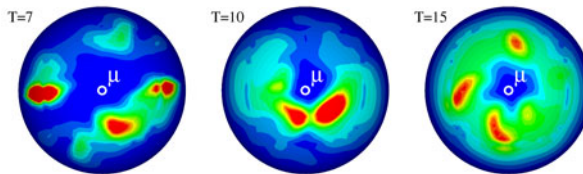


**Figure 4.** Hot spots on the star's surface at various times for our main case. The colors represent contours of the matter flux onto the star's surface, ranging from 0.2 (deep blue) to 3 (red).

with funnel streams, which flow towards the star's polar region from the part of the disk that is closest to the magnetic pole, and therefore usually rotate at approximately the angular velocity of the star. The gas at the base of the tongues tries to conserve angular momentum as it moves inwards, leading to an increase in its angular velocity, causing the tongues to curve to their right. The shape and number of the tongues change on the inner-disk dynamical timescale. The number of tongues varies between about 2 and 7.

Fig. 4 shows the hot spots on the star's surface for our main case at different times. We see that the spots are different from pure funnel-flow hot spots (Romanova *et al.* 2004, Kulkarni & Romanova 2005), and are significantly different from the simple polar-cap shape that is frequently assumed. Each tongue creates its own hot spots when it reaches the star's surface. Therefore, the shape, intensity, number and position of the spots change on the order of the inner-disk dynamical timescale.

In the following subsections, we investigate the dependence of the instability on different parameters, starting from the main case and varying one parameter at a time.

### 3.1. Dependence on the accretion rate

The accretion rate in our code is regulated by the viscosity coefficient  $\nu$  which is proportional to the  $\alpha$ -parameter (Shakura & Sunyaev 1973). The radial velocity of inward flow in the disk at a distance  $r$  from the star is  $v_r \approx \nu/r \approx \alpha c_s h/r$ , where  $h$  is the thickness of the disk and  $c_s$  is the sound speed. Thus the accretion rate through the disk is approximately proportional to  $\alpha$ :  $\dot{M} \approx 4\pi r h \rho v_r \sim \alpha$ .

We performed simulations for  $\alpha = 0.02, 0.03, 0.04, 0.06, 0.08, 0.1, 0.2, 0.3$ . At very small  $\alpha$  ( $\leq 0.03$ ), the instability does not appear. At larger  $\alpha$ , the instability appears, and when  $\alpha$  is increased, the instability starts earlier and more matter accretes through it. Fig. 5 shows equatorial slices of the plasma density distribution at different  $\alpha$  at  $t = 25$ . One can see that there are no tongues at  $\alpha = 0.02$ . The tongues are quite weak at  $\alpha = 0.04$ , but much stronger at larger  $\alpha$ , when more matter comes to the inner region of the disk, and the plasma density in the inner region of the disk is higher than in the low- $\alpha$  cases. This shows that increased accumulation of mass at the inner edge of the disk leads to enhancement of the instability, producing tongues with higher velocities that propagate deeper into the magnetosphere of the star. We should note that in spite

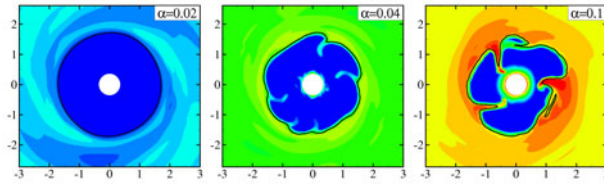


**Figure 5.** Plasma density distribution in the equatorial plane for different  $\alpha$  values at  $t = 25$ . The colors represent plasma density contours, ranging from red (highest) to deep blue (lowest). The solid line is the  $\beta = 1$  line.

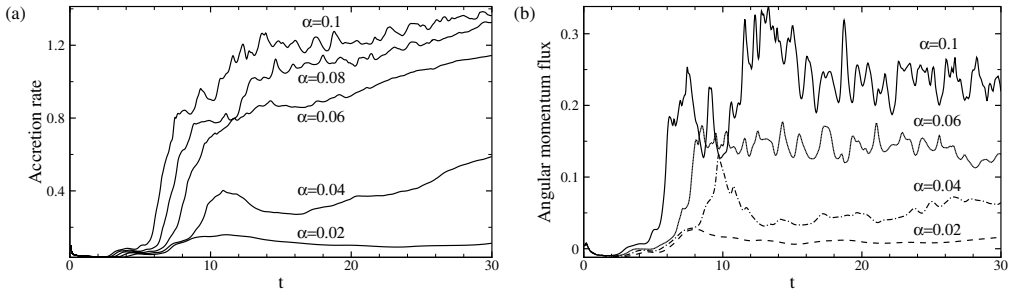


**Figure 6.** (a) Variation of the accretion rate onto the star’s surface with time, for different values of the  $\alpha$ -viscosity. Notice the sudden increase in the accretion rate for  $\alpha \geq 0.04$  between  $t = 5$  and  $t = 10$ , which occurs at the onset of the instability. (b) Variation with time of the angular momentum flux onto the star about the star’s rotational axis, for different values of the  $\alpha$ -viscosity.

of different conditions at the inner region of the disk (much higher density at larger  $\alpha$ ), the number and behaviour of the tongues is approximately the same in all cases.

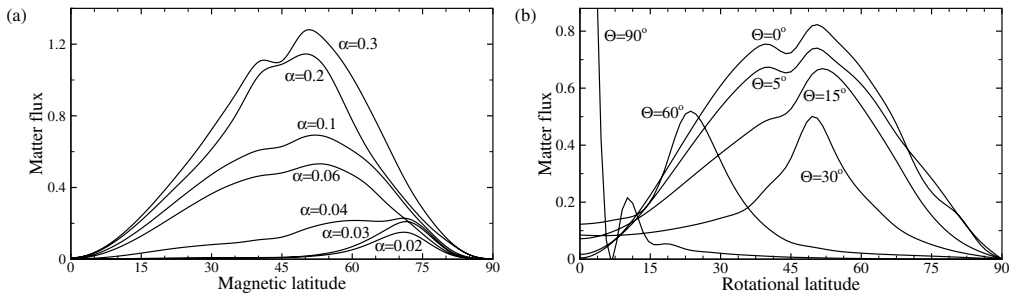
The accretion rate onto the star’s surface is higher during accretion through instability, as Fig. 6a shows. The increase the accretion rate with  $\alpha$  is not merely due to increase in the amount of matter transported inwards by the accretion disk. The sudden increase in accretion rate between  $t = 5$  and  $t = 10$  for the unstable cases ( $\alpha \geq 0.04$ ) occurs at the onset of the instability, which suggests that the instability, when present, is very efficient at transporting matter onto the star’s surface. The higher accretion rate is accompanied by a higher angular momentum flux to the star (Fig. 6b).

Fig. 7a shows the dependence on the magnetic latitude  $\theta$  of the matter flux onto the star’s surface, for different  $\alpha$ . For  $\alpha = 0.02$  and  $\alpha = 0.03$  the matter flux peaks at  $\theta \approx 73^\circ$  with a half-width of  $\approx 75^\circ - 65^\circ = 10^\circ$ . For  $\alpha = 0.06 - 0.1$ , the peak is at much lower latitudes,  $\theta \approx 53^\circ$ , with half-width  $\approx 70^\circ - 25^\circ = 45^\circ$ . It is surprising to see that at the largest viscosity coefficients,  $\alpha = 0.2$  and  $0.3$ , the hot spots do not move closer to equator, but have a maximum at  $\theta \approx 50^\circ$ , like for  $\alpha = 0.1$ .

### 3.2. Dependence on the misalignment angle

We find that the instability shuts off for  $\Theta \gtrsim 30^\circ$ . The reason for this is that for large misalignment angles ( $\Theta \gtrsim 30^\circ$ ), the magnetic poles are closer to the disk plane. Therefore, the gravitational energy barrier that the gas in the inner disk region has to overcome in order to form funnel flows is reduced, making funnel flows energetically more favourable.

Fig. 7b shows the accretion rate onto the star’s surface as a function of rotational latitude. When the accretion is through instability ( $\Theta \leq 30^\circ$ ), most of the matter accretes onto the mid-latitude ( $\theta \sim 50^\circ$ ) region of the star, independent of the misalignment angle.



**Figure 7.** (a) Dependence of the matter flux on the magnetic latitude for various  $\alpha$ . (b) Dependence of the matter flux on the rotational latitude for various  $\Theta$ .

### 3.3. Dependence on the grid resolution

The azimuthal width of the tongues is much larger than the size of our grid cells. This indicates that the instability is not an artefact of the coarseness of the grid. Nevertheless, to eliminate that possibility, we performed simulations at higher grid resolutions for comparison. We used the following resolutions:  $N_r \times N^2 = 72 \times 31^2, 100 \times 41^2$  and  $144 \times 61^2$ , where  $N_r$  and  $N$  are the number of grid cells in the radial and angular directions respectively in each of the six zones of the cubed sphere grid. The instability exists in all these cases, with similar tongue behaviour.

### 3.4. Possible perturbation mechanisms

Different sources of perturbation are expected at the disk-magnetosphere boundary in real accretion disks. There are always natural density and pressure inhomogeneities in the disk, which may act as perturbations. Also, if the magnetic and rotational axes are not aligned, there will always be some density enhancement near the disk foot-points of the funnel streams (Romanova *et al.* 2003, 2004). This would be a constant source of inhomogeneity in the disk. Another source of perturbation is associated with the magnetic field lines which are trapped inside the inner regions of the disk and are azimuthally wrapped by the disk matter. This leads to increase of magnetic energy in some parts of the disk and to partial expulsion of matter from these regions, and thus to inhomogeneous distribution of matter. This mechanism is expected to operate in real astronomical objects as well.

Concerning the role of the grid, it is unlikely, as noted above, that the discrete nature of the grid by itself leads to perturbations. But another perturbing element is the boundaries between the sectors of the cubed sphere grid. Four of these boundaries cross the disk. They produce initial density and pressure perturbations at the 5% level near the disk-magnetosphere boundary, and at even larger levels at larger distances from the star, where the grid is coarser. At later times these perturbations become less important. So at early times in the simulations, this boundary effect is the most important contributor to the perturbations. That is why we often see four tongues initially. However, at later times, we often observe anywhere between 2 and 7 tongues, which shows that there is no direct influence of these boundaries on the perturbations at later times.

### 3.5. Empirical conditions for the existence of the instability

For a given mass, radius, magnetic field strength and misalignment angle  $\Theta$  of the star, the presence of the instability is correlated with the star's rotation period  $P$  and the accretion rate  $\dot{M}$  at the star's surface. Fig. 8a shows the regimes of stable and unstable accretion in the  $\dot{M} - P$  plane for  $\Theta = 5^\circ$ , obtained empirically from the simulations.

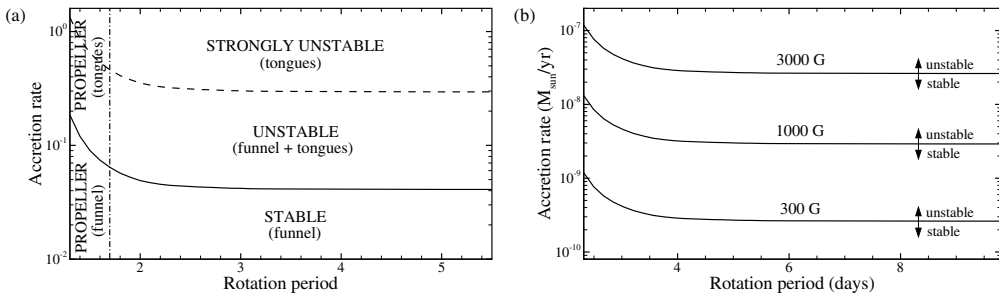


**Figure 8.** Nature of the accretion flow for different stellar rotation periods and accretion rates, (a) in dimensionless values, and (b) for a protostar with  $M = 0.8M_{\odot}$ ,  $R = 2R_{\odot}$ . The accretion rate is calculated at the star’s surface.

As noted in § 3.1, the presence of the instability is accompanied by high accretion rates. Also, unless the star rotates very rapidly (i.e., is close to the propeller stage), the presence of the instability is very weakly correlated with the rotation rate. The transition region between the regimes of pure funnel accretion and accretion solely through instabilities is fairly broad. In this region, simultaneous accretion through funnel streams and instability tongues is observed.

Fig. 8 is in dimensionless units, and therefore, as noted in § 2, can be used for a wide variety of physical situations with appropriately chosen reference values. The following are the reference values for an accretion disk around a protostar of mass  $M$ , radius  $R$  and surface magnetic field  $B$ :

$$P_0 = 1.8 \text{ days} \left( \frac{R}{2R_{\odot}} \right)^{3/2} \left( \frac{M}{0.8M_{\odot}} \right)^{-1/2} \tag{3.1}$$

$$\dot{M}_0 = 7 \times 10^{-8} M_{\odot} \text{ yr}^{-1} \left( \frac{B}{10^3 \text{ G}} \right)^2 \left( \frac{R}{2R_{\odot}} \right)^{5/2} \left( \frac{M}{0.8M_{\odot}} \right)^{-1/2} \tag{3.2}$$

Fig. 8b shows the boundary between the stable and unstable accretion regimes for protostars, for the fiducial values of mass and radius shown in equations 3.1 and 3.2, and different surface magnetic field strengths.

#### 4. Summary

Accretion through instabilities at the disk-magnetosphere interface occurs for a wide range of physical parameters. It results in tall, thin tongues of gas penetrating the magnetosphere and travelling in the equatorial plane. The tongues are very transient, and grow and rotate around the star on inner-disk dynamical timescales. The number of tongues at a given time is of the order of a few. Near the star, the tongues are threaded by the magnetic field lines, and form miniature funnel-like flows, which deposit matter much closer to the star’s equator than true funnel flows do. Each tongue produces its own hot spots on the star’s surface, and as a result, the hot spots also change on inner-disk dynamical timescales. The resulting light curves often show no clear periodicity. Sometimes, when a certain number of tongues dominate, we see quasi-periodic oscillations in the lightcurves.

The instability is associated with high accretion rates, and coexists with funnel flows for quite a broad range of accretion rates. Protostars with the fiducial mass, radius, surface magnetic fields and accretion rates of  $0.8M_{\odot}$ ,  $2R_{\odot}$ ,  $10^3 \text{ G}$  and  $10^{-8}M_{\odot} \text{ yr}^{-1}$  respectively are expected to be in this transition region.

The instability is suppressed if the misalignment angle  $\Theta$  between the star's rotation and magnetic axes is large ( $\Theta \gtrsim 30^\circ$ ). For  $\Theta \lesssim 30^\circ$ , when the accretion is through instability, the rotational latitude at which most of the accreting matter falls on the star is independent of the misalignment angle.

### Acknowledgements

This research was partially supported by the NSF grants AST-0507760 and AST-0607135, and NASA grants NNG05GL49G and NAG-513060. NASA provided access to high performance computing facilities.

### References

- Arons, J. & Lea, S. M. 1976, *ApJ* 207, 914  
 Elsner, R. F. & Lamb, F. K. 1977, *ApJ* 215, 897  
 Ghosh, P. & Lamb, F. K. 1978, *ApJ* 223, L83  
 Ghosh, P. & Lamb, F. K. 1979, *ApJ* 232, 259  
 Koldoba, A. V., Romanova, M. M., Ustyugova, G. V., & Lovelace, R. V. E. 2002, *ApJ* 576, L53  
 Kulkarni, A. K. & Romanova, M. M. 2005, *ApJ* 633, 349  
 Li, L.-X. & Narayan, R. 2004, *ApJ* 601, 414  
 Novikov, I., & Thorne, K. S. 1973, in: B. DeWitt and C. DeWitt (eds.), *Black Holes* (New York: Gordon and Breach), p. 409  
 Rastätter, L. & Schindler, K. 1999, *ApJ* 524, 361  
 Romanova, M. M., Ustyugova, G. V., Koldoba, A. V., & Lovelace, R. V. E. 2002, *ApJ*, 578, 420  
 Romanova, M. M., Ustyugova, G. V., Koldoba, A. V., Wick, J. V., & Lovelace, R. V. E. 2003, *ApJ* 595, 1009  
 Romanova, M. M., Ustyugova, G. V., Koldoba, A. V., & Lovelace, R. V. E. 2004, *ApJ* 610, 920  
 Shakura, N. I., & Sunyaev, R. A. 1973, *A&A* 24, 337  
 Spruit, H. C. & Taam, R. E. 1990, *A&A* 229, 475

### Discussion

MATT: How does the velocity of matter in the tongues compare with that in the funnels?

KULKARNI: They are of the same order.

JOHNS-KRULL: What is the filling factor of the hot spots during accretion through instability?

KULKARNI: The filling factor depends on the temperature that is taken to define the boundary of the hot spot. It is larger than for funnel flows, though.

HARRIES: Is the magnetic field on the star's surface weaker at the place where the tongues reach the star?

KULKARNI: No, because in the inner magnetosphere, the tongues are threaded by the stronger magnetic field and travel along the field lines.

FENDT: Is it possible that the instability seen in the simulations could be a result of diffusivity?

KULKARNI: That is unlikely, because our model assumes ideal MHD. The numerical diffusivity is relatively small, and decreases when the grid resolution is improved. Also, the instability progresses at much shorter timescales than the diffusive timescale.